Inhibition studies using anti-CYP antisera and chemical inhibitors

An immuno-inhibition study was conducted according to our previous report (Fujino et al. 2004a). Monkey hepatic microsomes were pre-incubated at room temperature for 20 min with 40–100 μl mg^{-1} microsomes of the goat antiserum for CYP1A2, CYP2A6, CYP2C8, CYP2C9, CYP2C19, CYP2D6, or CYP3A4. For control reactions, normal serum was used. Benzoflavone, quercetin, sulfaphenazole/gemfibrozil, tranylcypromine, qunidine and ketoconazole were used at 1–100 μM as relatively specific inhibitors of human CYP1A2, CYP2C8, CYP2C9, CYP2C19, CYP2D6 and CYP3A4, respectively. ^{14}C-pitavastatin or its lactone form was co-incubated at 2.5 μM as a substrate with these inhibitors. The inhibitory effect was estimated from the remaining amount of the substrates in the presence or absence of the inhibitors. The IC_{50} values were calculated by linear interpolation from the chemical inhibition study.

Identification of pitavastatin-metabolizing CYPs

To investigate the CYPs participating in pitavastatin metabolism, the partially purified recombinant CYP proteins for humans and monkeys were incubated with pitavastatin or its lactone form (both concentrations: 2.5 μM) for 30 min. Incubation with control microsomes from native insect cells was performed in parallel. The incubation conditions were the same as described above for the hepatic microsomes.

Kinetic analysis of pitavastatin and CYP2C model substrates

The CYP2C recombinant proteins and hepatic microsomes were used to perform the kinetic analysis of pitavastatin and several CYP2C model substrates in cynomolgus monkeys. The incubation conditions were essentially the same as the previous reports (Ludwig et al. 1998; Fujino et al. 2001; 2003). The Michaelis–Menten parameters of the apparent K_m and V_{max} were estimated by the Lineweaver–Burk reciprocal plots. The incubation was carried out for 30 min using the acid or lactone form at 1–80 μM as a substrate. The apparent K_m and V_{max} values were also calculated for 6α-hydroxypaclitaxel, 3-hydroxypaclitaxel, 4-hydroxytolbutamide, 2α-hydroxytestosterone, 16α-hydroxytestosterone and 6β-hydroxytestosterone. Paclitaxel, tolbutamide and testosterone were used at 2.5–40, 20–800 and 25–400 μM, respectively. Incubation with human hepatic microsomes was performed in parallel.

Analytical methods

The measurement of ^{14}C-labelled pitavastatin and its metabolites was performed according to the HPLC-radioluminography (RLG) method (Kimata et al. 1998) with some modifications. Briefly, using the HPLC systems (1100 Series, Agilent Technologies, Palo Alto, CA, USA) equipped with a fraction collector, the HPLC eluate was fractionated at an interval of 15 s up to 25 min into polystyrene flat-bottomed microplates (RLG plate Beta48, Toyobo, Osaka, Japan). The plates were allowed to stand for 12 h at room temperature for evaporation of the solvent. The analysis of 6α-hydroxypaclitaxel and 3-hydroxypaclitaxel was performed according to our previous report (Fujino et al. 2001). Aliquots (approximately 2 μl) of the supernatant were spotted onto the TLC plates (Silicagel $60F_{254}$, 20 × 20 cm; Merck, Darmstadt, Germany) and developed with toluene–acetone–formic acid (60:39:1, v/v/v) to 12 cm in a horizontal TLC chamber that was saturated with solvent vapour.

The analysis of testosterone metabolites was carried out as follows: supernatant was applied to TLC plates and developed with dichloromethane–acetone (4:1, v/v) to 16 cm. The measurement of 4-hydroxytolbutamide was performed according to a previous report (Ludwig et al. 1998). Briefly, the supernatant was spotted and developed with toluene–acetone–formic acid (60:39:1, v/v/v) to 10 cm. The RLG and TLC plates were dried and placed in contact with a phosphor imaging plate for 12 h. The amounts of unchanged drug and metabolites were determined using the BAS-2500 (Fuji Photo Film, Tokyo, Japan) system. The radioactive metabolites were positively identified by a comparison of retention times or R_f values using authentic unlabeled standard.

Results

Metabolic characterization of monkey CYP2Cs

We have previously reported the involvement of monkey CYP2C20, CYP2C43, CYP2C75 and CYP2C76 in the metabolism of model substrates for human CYPs such as paclitaxel, tolbutamide, *S*-mephenytoin and testosterone (Uno et al. 2006). In the current study, we further characterized the metabolic properties of CYP2Cs by kinetic analysis using monkey and human hepatic microsomes (Table I) and the recombinant proteins for the monkey CYP2Cs (Table II).

We first evaluated the metabolic constants for paclitaxel, tolbutamide, *S*-mephenytoin and testosterone using human and monkey hepatic microsomes (Table I). The apparent K_m values for tolbutamide 4-hydroxylation in humans and monkeys were 130 and 866 μM, respectively, indicating a weaker affinity for tolbutamide metabolism in monkeys than humans. In contrast, the apparent V_{max} for *S*-mephenytoin 4-hydroxylation was 41 and 167 pmol min^{-1} mg^{-1} protein in human and monkey hepatic microsomes, respectively, suggesting a higher activity for *S*-mephenytoin 4-hydroxylation in monkeys than humans.

To identify which CYPs are responsible for the metabolism of each substrate in monkeys, a similar analysis was carried out using the recombinant monkey CYP2Cs (Table II).

Table I. Kinetic constants of testosterone, tolbutamide, paclitaxel and *S*-mephenytoin metabolism in human and monkey hepatic microsomes.

Species	Substrate	Metabolite	Km (μM)	Vmax (pmol min^{-1} mg^{-1} protein)
Human	Testosterone	6β-hydroxy testosterone	109	4535
		2α-hydroxy testosterone	105	363
		16α-hydroxy testosterone	60.0	140
	Tolbutamide	4-hydroxy tolbutamide	130	169
	Paclitaxel	6α-hydroxy paclitaxel	6.3	83.0
		3-hydroxy paclitaxel	9.7	101
	S-mephenytoin	4-hydroxy mephenytoin	97.2	41.0
Monkey	Testosterone	6β-hydroxy testosterone	136	5643
		2α-hydroxy testosterone	687	3420
		16α-hydroxy testosterone	154	601
	Tolbutamide	4-hydroxy tolbutamide	866	497
	Paclitaxel	6α-hydroxy paclitaxel	9.6	60.0
		3-hydroxy paclitaxel	16.1	128
	S-mephenytoin	4-hydroxy mephenytoin	75.8	167

Data are derived from duplicate determinations.

Table II. Kinetic constants of paclitaxel, tolbutamide and testosterone metabolism in the recombinant proteins for monkey CYP2Cs.

Substrate	Enzyme	Metabolite	*K*m (μM)	V_{max} (pmol min^{-1} $nmol^{-1}$ P450)
Paclitaxel	CYP2C20	6α-Hydroxy paclitaxel	2.2	15.1
		3-Hydroxy paclitaxel	–	–
Tolbutamide	CYP2C75	4-Hydroxy tolbutamide	775	863
	CYP2C76	4-Hydroxy tolbutamide	866	283
Testosterone	CYP2C75	6β-Hydroxy testosterone	–	–
		2α-Hydroxy testosterone	34.0	864
		16α-Hydroxy testosterone	–	–
	CYP2C76	6β-Hydroxy testosterone	–	–
		2α-Hydroxy testosterone	47.4	56.1
		16α-Hydroxy testosterone	42.4	152

Data are derived from duplicate determinations.

The apparent K_m values for paclitaxel 6α-hydroxylation in monkey hepatic microsomes and CYP2C20 were 9.6 and 2.2 μM, respectively. For tolbutamide metabolism, the apparent K_m values for tolbutamide 4-hydroxylation in monkey hepatic microsomes, CYP2C75 and CYP2C76 were 866, 755 and 866 μM, respectively. For testosterone metabolism, the apparent K_m values for 2α-hydroxytestosterone in monkey hepatic microsomes, CYP2C75 and CYP2C76 were 687, 34.0 and 47.4 μM, respectively. Moreover, the apparent K_m values for 16α-hydroxytestosterone in monkey hepatic microsomes and CYP2C76 were 154 and 42.4 μM, respectively. These K_m values suggest that CYP2C20 is critically involved in the metabolism of paclitaxel, whereas CYP2C75 and CYP2C76 play major roles in the metabolism of tolbutamide and testosterone, respectively. However, the metabolic activity toward tolbutamide was 2.2-fold lower in monkeys than humans. We conclude that CYP2C76 apparently catalyses a different metabolic pattern from any other monkey CYP2Cs, but this does not explain the species difference observed in the metabolism of model substrates for human CYP2Cs between monkeys and humans. To show clearly the involvement of CYP2C76 in the species difference in drug metabolism, we therefore investigated pitavastatin metabolism.

Metabolism of pitavastatin in hepatic microsomes from monkey and human hepatic microsomes

NADPH- and UGT-mediated metabolic clearance of pitavastatin was determined using monkey and human hepatic microsomes (Table III). A larger clearance of the acid and/or lactone forms was seen in monkeys compared with humans. In addition, the appearance of the acid form hydrolysed from the lactone form was approximately 30% of the total amount in humans as compared with monkey hepatic microsomes (data not shown).

NADPH-mediated metabolism of the acid and lactone forms of pitavastatin is shown in Figure 1. The acid form underwent hydroxylation in monkey microsomes to afford at least two metabolic products, M-13 and M-14. In the case of the lactone form, several metabolites such as M-3, M-13 and M-14 were detected including unknown metabolites. Moreover, NADPH- and UGT-mediated metabolism were negligible in renal and intestinal microsomes of monkeys (data not shown).

Table III. Metabolic clearance of pitavastatin in monkey and human hepatic microsomes.

	CL_{int} ($\mu l\,min^{-1}\,mg^{-1}$ protein)		
	Acid form		Lactone form
Species	NAPDH-mediated	UGT-mediated	NAPDH-mediated
Monkey	17.1	62.8	33.2
Human	3.3	5.6	3.5

Data are derived from duplicate determinations.

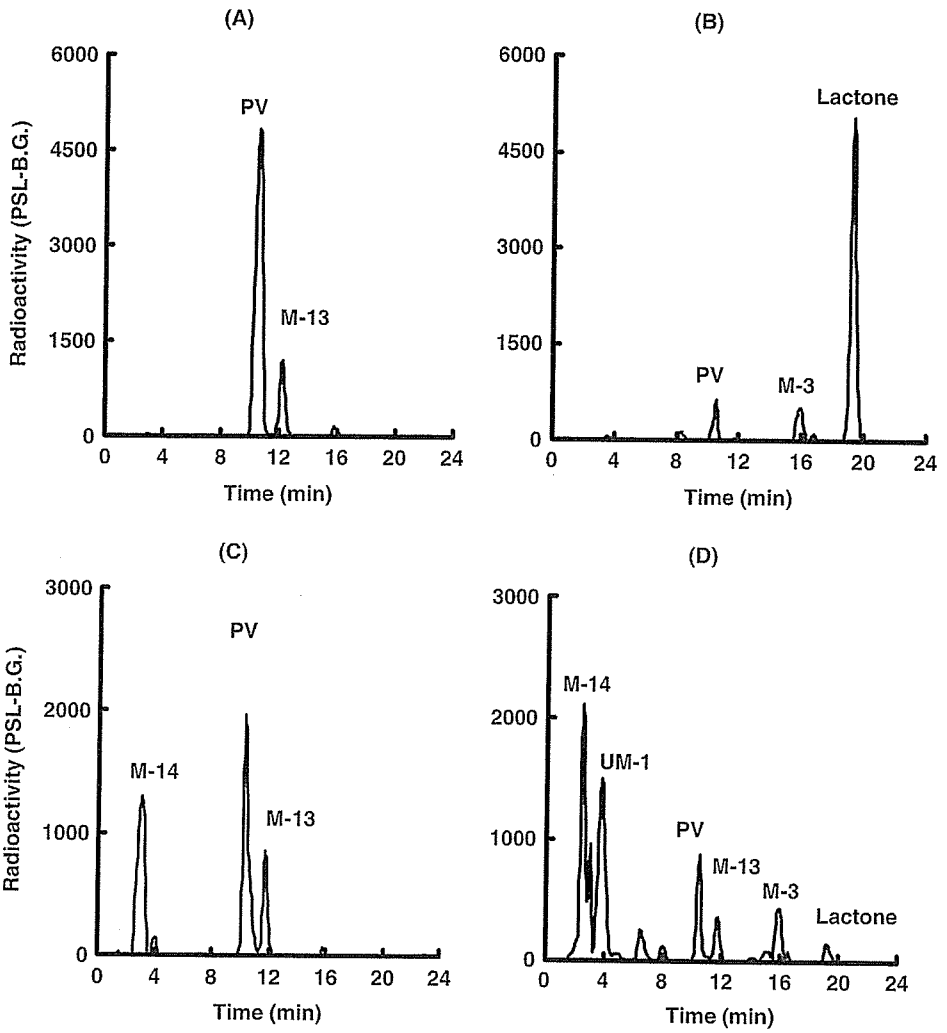

Figure 1. HPLC radiochromatograms of pitavastatin and its metabolites in human and monkey hepatic microsomes. The metabolic assays were performed with the acid (A and C) and lactone (B and D) forms of pitavastatin using human (upper) and monkey (lower) hepatic microsomes as described in the Materials and methods section. Results are representative of two separate experiments with each microsome sample.

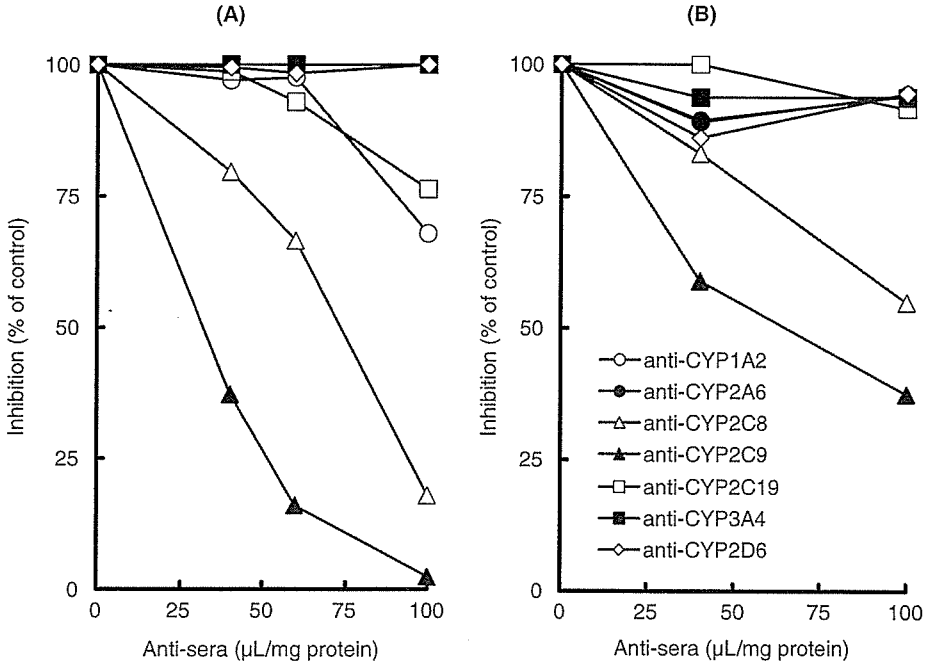

Figure 2. Immuno-inhibition of pitavastatin metabolism in monkey hepatic microsomes. Inhibition of the acid (A) and lactone (B) forms of pitavastatin was carried out using the antibodies for human CYP1A2, CYP2A6, CYP2C8, CYP2C9, CYP2C19, CYP2D6, or CYP3A4. Monkey hepatic microsomes were pre-incubated at room temperature for 20 min with 100 μl mg^{-1} microsomes of goat antiserum for the CYPs. The acid or lactone form (2.5 μM) was then added and co-incubated in the reaction mixture. The inhibitory effect was estimated from the remaining pitavastatin and its lactone form in the presence and absence of the antibodies. Data are from duplicate experiments.

Inhibition of pitavastatin metabolism in monkey hepatic microsomes by antibodies to human CYPs and typical CYP inhibitors

The involvement of CYPs in the metabolism of the acid and lactone forms of pitavastatin was investigated in monkey hepatic microsomes using antisera and chemical inhibitors of human CYPs. Among antisera for human CYP1A2, CYP2A6, CYP2C8, CYP2C9, CYP2C19, CYP2D6 and CYP3A4 used with the acid form, only anti-CYP2C8 or CYP2C9 antisera strongly inhibited metabolite formation in monkey microsomes (Figure 2A). For the lactone form, a moderate or strong inhibition was observed in monkey microsomes by anti-CYP2C8 or CYP2C9 antisera, respectively (Figure 2B). These results indicate that monkey CYP2Cs are substantially involved in pitavastatin metabolism; however, critical site- or substrate-selective differences exist in the activities of CYP2Cs between monkeys and humans. Next, the inhibitory effects of several chemical inhibitors of human CYPs on the metabolism of pitavastatin were determined using benzoflavone, tranylcypromine, quercetin, sulfaphenazole, ketoconazole, gemfibrozil and quinidine (Table IV). For the acid form, the IC_{50} values for tranylcypromine and ketoconazole were 22 and 64 μM, respectively, indicating the inhibitory effect of these inhibitors. In contrast, the metabolism of the lactone form was inhibited by benzoflavone and ketoconazole because the IC_{50} values for these

Table IV. Chemical inhibition of pitavastatin metabolism in monkey hepatic microsomes.

	IC_{50} (μM)	
Inhibitors	Acid form	Lactone form
Benzoflavone	>100	29
Tranylcypromine	22	95
Quercetin	>100	>100
Sulfaphenazole	>100	>100
Ketoconazole	64	25
Gemfibrozil	>100	>100
Quinidine	>100	>100

Data are derived from duplicate determinations

inhibitors were 29 and 25 μM, respectively. A substantial difference in the inhibitory profiles of these chemical inhibitors supports the involvement of different CYP2Cs in the metabolism of each form of pitavastatin.

Role of CYPs in the metabolism of pitavastatin in humans and monkeys

The catalytic roles of each recombinant CYP on the metabolism of the acid and lactone forms of pitavastatin were examined using the recombinant proteins for human CYP1A2, CYP2A6, CYP2C8, CYP2C9, CYP2C19, CYP2E1 and CYP3A4 (Figure 3A). For monkeys, CYP2C20, CYP2C43, CYP2C75 and CYP2C76 were used (Figure 3B). The monkey CYP2E and CYP3A subfamilies were not included because the recombinant proteins for these CYPs were not available. In humans, CYP2C8 and CYP2C9 were shown to catalyse the metabolism of the acid form. In contrast, CYP3A4, not CYP2Cs, supported the metabolism of the lactone form. In monkeys, the acid form was metabolized by CYP2C43 and CYP2C75 while the lactone form was by CYP2C43, CYP2C75 and CYP2C76. CYP2C20 was not involved in pitavastatin metabolism. These observations indicate a major role of CYP2C76 in the metabolism of the lactone form, for which CYP3A4 is essential in humans, raising the possibility of CYP2C76 in the species difference in pitavastatin metabolism.

Kinetic analysis of pitavastatin metabolism

The metabolism of pitavastatin in monkey hepatic microsomes and the recombinant monkey CYP2Cs followed Michaelis–Menten kinetics as demonstrated by Lineweaver–burk plots, and the curves were all linear (data not shown). In the metabolism of the acid form, the apparent K_m of hepatic microsomes, CYP2C43 and CYP2C75 for M-13 formation were 13.5, 129.1 and 8.8 μM, respectively, while the apparent K_m of hepatic microsomes and CYP2C75 for M-14 formation was 13.4 and 1.2 μM, respectively (Table V). In the case of the lactone form, the apparent K_m for M-13 formation was 7.1 μM for recombinant CYP2C75. On the other hand, CYP2C76 was involved in M-3, M-13 and M-14 formation with apparent K_m values of 4.5, 24.9 and 36.6 μM, respectively. These results suggest that CYP2C75 is critically involved in the metabolism of the acid form and for M-13 formation from the lactone form. In contrast, CYP2C76 plays a major role in the formation of the several metabolites with relatively low K_m values.

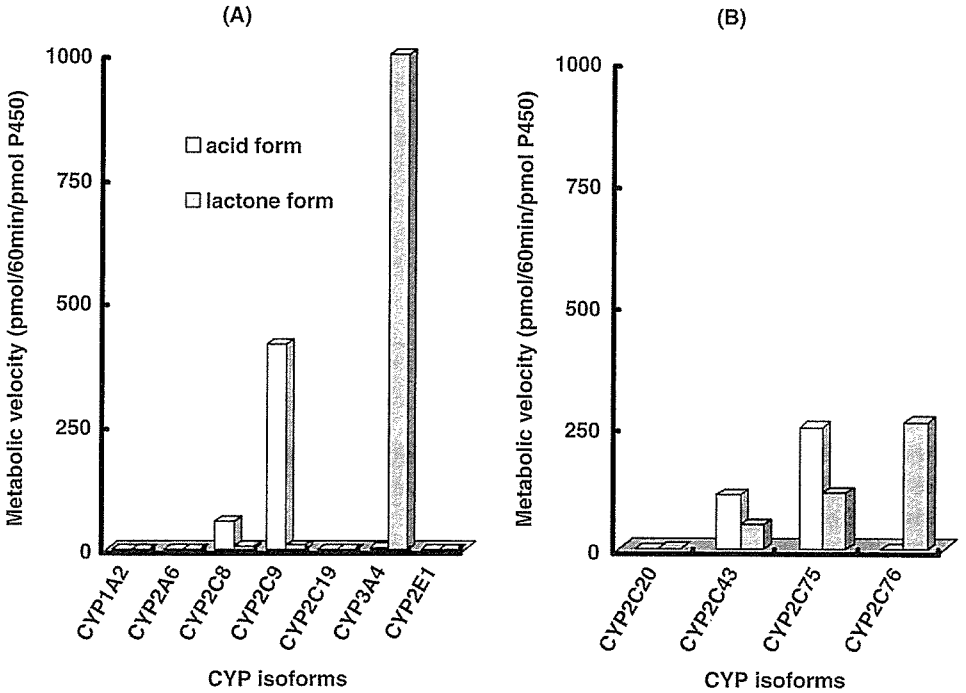

Figure 3. Identification of CYPs involved in pitavastatin metabolism in humans (A) and monkeys (B). Recombinant monkey CYP2C proteins were expressed in *E. coli* and the metabolic assays were performed using the monkey or human CYP proteins as described in the Materials and methods section. Results are based on duplicate determinations.

Table V. Kinetic constants of pitavastatin metabolism in monkey hepatic microsomes and the recombinant proteins for monkey CYP2Cs.

Pitavastatin	Enzyme	Metabolite	Km (μM)	V_{max}* (pmol min^{-1} $nmol^{-1}$ P450)
Acid form	Hepatic microsomes	M-13	13.5	106.7
		M-14	13.4	81.1
	CYP2C43	M-13	129.1	1809
	CYP2C75	M-13	8.8	257.7
		M-14	1.2	7.7
Lactone form	CYP2C75	M-13	7.1	23.5
	CYP2C76	M-3	4.5	96.4
		M-13	24.9	129.1
		M-14	36.6	26.9

*V_{max} for hepatic microsomes is expressed as pmol min^{-1} mg^{-1} protein. Data are derived from duplicate determinations.

Discussion

Monkey CYP2C76, which does not have an orthologue in humans, has metabolic properties different from other monkey CYP2Cs such as CYP2C20, CYP2C43 and

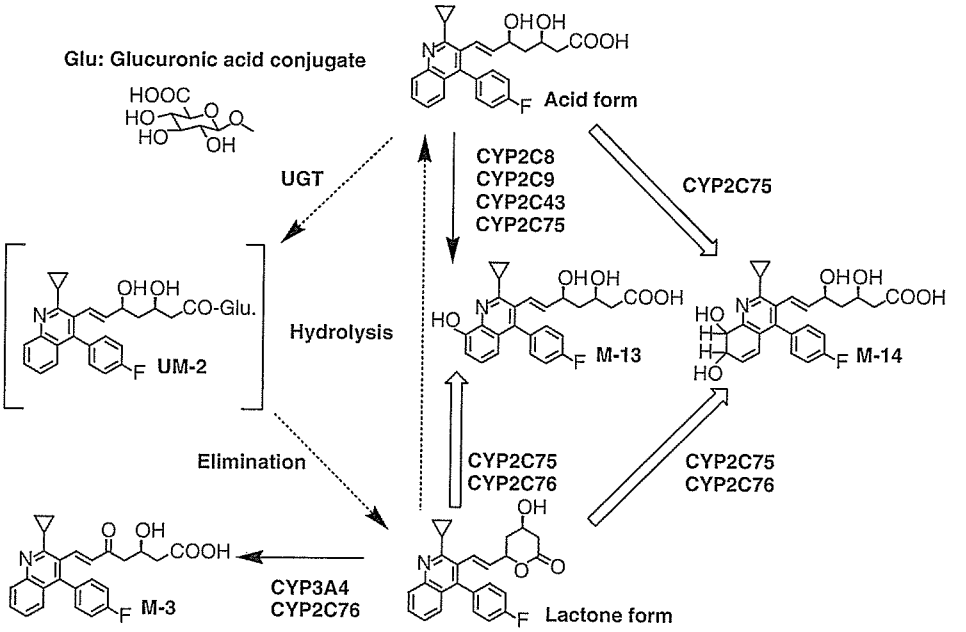

Figure 4. Postulated metabolic pathways of pitavastatin in monkeys and humans. Solid lines indicate common metabolic pathways and dotted lines are the CYP-independent metabolic pathways in monkeys and humans. The block lines indicate the monkey-specific pathways of pitavastatin metabolism.

CYP2C75 (Uno et al. 2006). This species specificity and functional uniqueness strongly suggests that CYP2C76 could be responsible for the some difference in drug metabolism between monkeys and humans. The current study first investigated whether CYP2C76 accounts for the species difference in the metabolism of model substrates for human CYP2Cs. The involvement of CYP2C76, however, could not be clearly indicated for species differences seen in tolbutamide or *S*-mephenytoin metabolism between monkeys and humans. Therefore, we decided to investigate pitavastatin metabolism, in which the different metabolic processes have been noted for the acid and lactone forms in monkeys as compared to humans.

CYP2Cs are substantially involved in pitavastatin metabolism, as evidenced by inhibition studies. Anti-CYP2C9 antisera showed a potent inhibition, whereas chemical inhibitors specific for human CYP2C8/9 such as quercetin, sulphafenazole and gemfibrozil, did not inhibit the metabolism of either form in monkey hepatic microsomes. These results indicate that monkey CYP2Cs play an important role in pitavastatin metabolism; however, differences exist in site- or substrate-selectivity for the activities of CYP2Cs between monkeys and humans. On the other hand, a substantial inhibition of the acid form was noted in the presence of tranylcypromine, a human CYP2C19 inhibitor. Moreover, benzoflavone and ketoconazole, which selectively inhibit human CYP1A2 and CYP3A4, respectively, showed a potent inhibition for the lactone form. These results suggest that different CYP2Cs are involved in the metabolism of each form of pitavastatin.

Analysis using recombinant proteins also indicated the involvement of CYP2Cs in pitavastatin metabolism in monkeys, namely CYP2C75 and CYP2C76, but not CYP2C20. Moreover, the metabolic properties mediated by these monkey CYP2Cs exhibited a substantial difference in metabolite formation and metabolic clearance of pitavastatin as compared with those of human CYP2Cs. As proposed in Figure 4, monkey CYP2C75 is

critically involved in the overall formation of M-13 and M-14 with relatively low K_m values. CYP2C76 is mainly involved in the metabolism of the lactone form to generate M-3, M-13 and M-14. In other species, the lactone form is metabolized by CYP3As such as CYP3A4 in humans, CYP3A2 in rats, or CYP3A12 in dogs (data not shown). These results clearly indicate that CYP2C76 is involved in the species difference of pitavastatin metabolism between monkeys and humans.

Considering the apparent involvement of CYP2C76 in the species difference between monkeys and humans in drug metabolism, identification and characterization of monkey CYPs responsible for drug metabolism are an inevitable task to better understand species difference between monkeys and humans. The unidentified species–specific CYPs other than CYP2C76, if any, could also result in the difference of in drug metabolism between monkeys and humans. Two different CYP2Ds in common marmosets, CYP2D19 and CYP2D30, show different metabolic properties, although it is not known whether these CYP2Ds are encoded by different genes (Hichiya et al. 2004). Based on this report, it was considered that these CYP2Ds, if present in the genome as distinct genes, could be responsible for species differences between monkeys and humans, considering that only CYP2D6 is functional among the three human CYP2D genes identified to date. The evolutionary closeness of cynomolgus monkeys to common marmosets raises the possibility that cynomolgus monkeys might also have more than one CYP2D6-related protein. By immunoblotting studies, two distinct protein bands were detected which are immuno-reactive with human CYP2D6 antibodies in cynomolgus monkey liver (Weaver et al. 1999), making this possibility more likely.

Eliminating the function of CYP2C76 in monkeys is expected to lead to a metabolic pattern even more similar to humans. Inactivation of the gene itself has been accomplished by gene-targeting in mice, but has not been successfully applied to non-human primate species including cynomolgus monkeys (Norgren, 2004). An alternative way is to identify functionally null or defective mutations, which have been reported for the human CYP genes including CYP2C8, CYP2C9, CYP2C19 (for details, see http://www.imm.ki.se/CYPalleles/). Similar mutations were also identified in dogs, which are frequently used in the preclinical studies of drug metabolism. A nonsense mutation (C1117T) in CYP1A2 decreases the production of the intact protein, leading to the phenotype of poor metabolizer (Mise et al. 2004). Moreover, >10% of 149 beagle dogs analysed were homozygotes for this mutation (Tenmizu et al. 2004). With the relatively high frequency of such defective or null alleles, such alleles might be easily identified in CYP2C76 and utilized to establish better model animals homozygous with the alleles in monkeys.

In conclusion, we have provided evidence that CYP2C76 is responsible for the species difference in the metabolism of pitavastatin. Using monkey CYP2C recombinant proteins, further investigations will elucidate the involvement of CYP2C76 for species difference between monkeys and humans in CYP2C-dependent metabolism of various drugs. Further identification and characterization of monkey-specific drug-metabolizing enzymes should help to understand more fully species difference in drug metabolism between monkeys and humans and to extrapolate the data obtained using monkeys to humans.

Acknowledgements

The authors are grateful to Mr Junji Kojima, Mr Tsuyoshi Saito and Mr Shin-ichiro Ogawa for their technical assistant and invaluable suggestions.

References

Aoki T, Yoshinaka Y, Yamazaki H, Suzuki H, Tamaki T, Sato F, Kitahara M, Saito Y. 2002. Triglyceride-lowering effect of pitavastatin in a rat model of postprandial lipemia. European Journal of Pharmacology 444:107–113.

Bogaards JJP, Bertrand M, Jackson P, Oudshoorn MJ, Weaver RJ, Bladeren PJ, Walther B. 2000. Determining the best animal model for human cytochrome P450 activities: A comparison of mouse, rat, rabbit, dog, micropig, monkey and man. Xenobiotica 12:1131–1152.

Daigo S, Takahashi Y, Fujieda M, Ariyoshi N, Yamazaki H, Koizumi W, Tanabe S, Saigenji K, Nagayama S, Ikeda K, Nishioka Y, Kamataki T. 2002. A novel mutant allele of the CYP2A6 gene (CYP2A6*11) found in a cancer patient who showed poor metabolic phenotype towards tegafur. Pharmacogenetics 12:299–306.

Fujino H, Kojima J, Yamada Y, Kanda H, Kimata H. 1999a. Studies on the metabolic fate of NK-104, a new inhibitor of HMG-CoA reductase (4): Interspecies variation in laboratory animals and humans. Xenobiotic Metabolism and Disposition 14:79–91.

Fujino H, Saito T, Tsunenari Y, Kojima J, Sakaeda T. 2004b. Metabolic properties of the acid form and lactone form of HMG-CoA reductase inhibitors. Xenobiotica 34:961–971.

Fujino H, Saito T, Tsunenari Y, Kojima J. 2004a. Effect of gemfibrozil on the metabolism of pitavastatin – Determining the best animal model for human CYP and UGT activities. Drug metabolism and Drug Interactions 20:25–42.

Fujino H, Yamada I, Hirano M, Yoneda M. 1999b. Studies on the metabolic fate of NK-104, a new inhibitor of HMG-CoA reductase (5): In vitro metabolism and plasma protein binding in animals and human. Xenobiotic Metabolism and Disposition 14:415–424.

Fujino H, Yamada I, Shimada S, Yoneda M, Kojima J. 2003. Metabolic fate of pitavastatin, a new inhibitor of HMG-CoA reductase: Human UDP-glucuronosyltransferase enzymes involved in lactonization. Xenobiotica 33:27–41.

Fujino H, Yamada I, Shimada S, Yoneda M. 2001. Simultaneous determination of taxol and its metabolites in microsomal samples by a simple thin-layer chromatography radioactivity assay. Journal of Chromatography 757:143–150.

Hichiya H, Kuramoto S, Yamamoto S, Shinoda S, Hanioka N, Narimatsu S, Asaoka K, Miyata A, Iwata S, Nomoto M, Satoh T, et al. 2004. Cloning and functional expression of a novel marmoset cytochrome P450 2D enzyme, CYP2D30: Comparison with the known marmoset CYP2D19. Biochemical Pharmacology 68:165–175.

Iwata H, Fujita K, Kushida H, Suzuki A, Konno Y, Nakamura K, Fujino A, Kamataki T. 1998. High catalytic activity of human cytochrome P450 co-expressed with human NADPH-cytochrome P450 reductase in Escherichia coli. Biochemical Pharmacology 55:1315–1325.

Jacqz E, Billante C, Moysan F, Mathieu H. 1988. The non-human primate: A possible model for human genetically determined polymorphisms in oxidative drug metabolism. Molecular Pharmacology 34:215–217.

Kimata H, Fujino H, Koide T, Yamada Y, Tsunenari Y, Yonemitsu M. 1998. Studies on the metabolic fate of NK-104, a new inhibitor of HMG-CoA reductase (1): Absorption, distribution, metabolism and excretion in rats. Xenobiotic Metabolism and Disposition 13:484–498.

Kojima J, Fujino H, Yosimura M, Morikawa H, Kimata H. 1999. Simultaneous determination of NK-104 and its lactone in biological samples by column-switching high-performance liquid chromatography with ultraviolet detection. Journal of Chromatography (B) 724:173–180.

Komori M, Kikuchi O, Sakuma T, Funaki J, Kitada M, Kamataki T. 1992. Molecular cloning of monkey liver cytochrome P-450 cDNAs: Similarity of the primary sequences to human cytochromes P-450. Biochimica et Biophysica Acta 1171:141–146.

Ludwig E, Wolfinger H, Ebner T. 1998. Assessment of microsomal tolbutamide hydroxylation by a simple thin-layer chromatography radioactivity assay. Journal of Chromatography 707:347–350.

Matsunaga T, Ohmori S, Ishida M, Sakamoto Y, Nakasa H, Kitada M. 2002. Molecular cloning of monkey CYP2C43 cDNA and expression in yeast. Drug Metabolism and Pharmacokinetics 17:117–124.

Mise M, Hashizume T, Matsumoto S, Terauchi Y, Fujii T. 2004. Identification of non-functional allelic variant of CYP1A2 in dogs. Pharmacogenetics 14:769–773.

Narimatsu S, Kobayashi N, Masubuchi Y, Horie T, Kakegawa T, Kobayashi H, Hardwick JP, Gonzalez FJ, Shimada N, Ohmori S, Kitada M, et al. 2000. Species difference in enantioselectivity for the oxidation of propranolol by cytochrome P450 2D enzymes. Chemico-Biological Interactions 15:73–90.

Nedelcheva V, Gut I. 1994. P450 in the rat and man: Methods of investigation, substrate specificities and relevance to cancer. Xenobiotica 24:1151–1175.

Norgren Jr RB. 2004. Creation of non-human primate neurogenetic disease models by gene targeting and nuclear transfer. Reproductive Biology and Endocrinology 2:40.

Ohi H, Toratani S, Komori M, Miura T, Kitada M, Kamataki T. 1989. Comparative study of cytochrome P-450 in liver microsomes. A form of monkey cytochrome P-450, P-450-MK1, immunochemically cross-reactive with antibodies to rat P-450-male. Biochemical Pharmacology 38:361–365.

Prueksaritanont T, Gorham LM, Hochman JH, Tran LO, Vyas KP. 1996. Comparative studies of drug-metabolizing enzymes in dog, monkey, and human small intestines, and in Caco-2 cells. Drug Metabolism and Disposition 24:634—642.

Sharer JE, Shipley LA, Vandenbranden MR, Binkley SN, Wrighton SA. 1995. Comparisons of phase one and phase two in vitro hepatic enzyme activities of human, dog, rhesus monkey, and cynomolgus monkey. Drug Metabolism and Disposition 23:1231–1241.

Stevens JC, Shipley LA, Cashman JR, Vandenbranden M, Wrighton SA. 1993. Comparison of human and rhesus monkey in vitro phase I and phase II hepatic drug metabolism activities. Drug Metabolism and Disposition 21:753–760.

Suzuki H, Aoki T, Tamaki T, Sato F, Kitahara M, Saito Y. 1999. Hypolipidemic effect of NK-104, a potent HMG-CoA reductase inhibitor, in guinea pigs. Atherosclerosis 146:259–270.

Tenmizu D, Endo Y, Noguchi K, Kamimura H. 2004. Identification of the novel canine CYP1A2 1117C > T SNP causing protein deletion. Xenobiotica 34:835–846.

Uno Y, Fujino H, Kito G, Kamataki T, Nagata R. 2006. CYP2C76, a novel CYP in cynomolgus monkey, is a major CYP2C in liver, metabolizing tolbutamide and testosterone. Molecular Pharmacology 70:477–486.

Weaver RJ, Dickins M, Burke MD. 1999. A comparison of basal and induced hepatic microsomal cytochrome P450 monooxygenase activities in the cynomolgus monkey (Macaca fascicularis) and man. Xenobiotica 29:467–482.

Weaver RJ, Thompson S, Smith G, Dickins M, Elcombe CR, Mayer RT, Burke MD. 1994. A comparative study of constitutive and induced alkoxyresorufin O-dealkylation and individual cytochrome P450 forms in cynomolgus monkey (Macaca fascicularis), human, mouse, rat and hamster liver microsomes. Biochemical Pharmacology 47:763–773.

Yamada I, Fujino H, Shimada S, Kojima J. 2003. Metabolic fate of pitavastatin, a new inhibitor of HMG-CoA reductase: Similarities and difference in the metabolism of pitavastatin in monkeys and humans. Xenobiotica 33:789–803.

Available online at www.sciencedirect.com
ScienceDirect
Molecular Genetics and Metabolism 90 (2007) 58–63
Molecular Genetics and Metabolism
www.elsevier.com/locate/ymgme

Stop codon mutations in the flavin-containing monooxygenase 3 (*FMO3*) gene responsible for trimethylaminuria in a Japanese population

Hiroshi Yamazaki [a,b,*], Haruka Fujita [a], Takaaki Gunji [b], Jun Zhang [c], Tetsuya Kamataki [b], John R. Cashman [c], Makiko Shimizu [a]

[a] *Laboratory of Drug Metabolism and Pharmacokinetics, Showa Pharmaceutical University, Machida, Tokyo 194-8543, Japan*
[b] *Graduate School of Pharmaceutical Sciences, Hokkaido University, Sapporo 060-0812, Japan*
[c] *Human BioMolecular Research Institute, San Diego, CA 92121, USA*

Received 15 June 2006; received in revised form 11 August 2006; accepted 11 August 2006
Available online 25 September 2006

Abstract

The reduced capacity of flavin-containing monooxygenase 3 (FMO3) to *N*-oxidize trimethylamine (TMA) is believed to cause a metabolic disorder. The aim of this study was to investigate the inter-individual variations of FMO3. Genomic DNA of case subjects that showed only 10–20% of FMO3 metabolic capacity among self-reported trimethylaminuria Japanese volunteers was sequenced. Functional analysis of recombinant FMO3 proteins was also performed. One homozygote for a novel single nucleotide substitution causing a stop codon at Arg500 was observed. The biological parents of this Proband A were heterozygous and showed >90% TMA *N*-oxygenation metabolic capacity. Another Proband B had the Arg500Stop and Cys197Stop codons. The TMA *N*-oxygenation metabolic capacities of the father and brother of this Proband B were apparently observed by possessing Arg205Cys mutant that coded for decreased TMA *N*-oxygenase. Recombinant Arg500Stop FMO3 cDNA expressed in *Escherichia coli* membranes and a series of highly purified truncation mutants at different positions of the C-terminus of FMO3 showed no detectable functional activity toward typical FMO3 substrates. The results suggest that individuals homozygous for either of the nonsense mutations, Arg500Stop and/or Cys197Stop alleles, in the *FMO3* gene can possess abnormal TMA *N*-oxygenation.
© 2006 Elsevier Inc. All rights reserved.

Keywords: Flavin-containing monooxygenase; Fish-like odor syndrome; Trimethylamine; Truncated FMO3; Japanese; Trimethylaminuria

Introduction

The flavin-containing monooxygenase (FMO, EC 1.14.13.8) is an NADPH-dependent enzyme that catalyzes the oxygenation of a wide variety of nucleophilic compounds containing sulfur, nitrogen or phosphorus atoms [1,2]. To date, eleven *FMO* genes have been identified in humans (*FMO1* to *FMO11p*) but only FMO1–5 are functionally active [3]. FMO3 is considered a prominent functional form expressed in adult human liver although FMO5 is also present [4,5]. In humans, a 20-fold inter-individual variation in FMO3 expression levels have been reported [6,7]. FMO3 may also play a role in processing some types of drugs such as the anticancer drug tamoxifen, the pain medication codeine, the antifungal drug ketoconazole, the addictive chemical nicotine found in tobacco, and diet-derived trimethylamine (TMA) [1,2]. Wild-type human FMO3 has 532 amino acids but there are genetic polymorphisms in the *FMO3* gene that code for naturally truncated forms that have no or almost no detectable amount of functional enzymatic activity [1,8–10]. Mutations in the *FMO3* gene are summarized in a Web-database using systematic and trivial names [8].

* Corresponding author. Fax: +81 42 721 1406.
E-mail address: hyamazak@ac.shoyaku.ac.jp (H. Yamazaki).

1096-7192/$ - see front matter © 2006 Elsevier Inc. All rights reserved.
doi:10.1016/j.ymgme.2006.08.008

Trimethylaminuria, or fish-like odor syndrome, is a genetic disease characterized by excretion of excessive unmetabolized TMA [11,12]. Individuals suffering from trimethylaminuria have a decreased capacity to oxygenate free malodorous TMA to non-odorous trimethylamine *N*-oxide (TMAO) by the FMO3 [13,14] and this is the case for individuals with causative nonsense *FMO3* gene mutations found in North American and European populations [15,16]. Unpleasant and/or pungent malodor caused by excess TMA present in various bodily fluids of some affected individuals may lead to profound social problems [11,12].

Due to its strong linkage with trimethylaminuria, considerable work has been done related to the contribution of genetic polymorphisms of the *FMO3* gene of the coding region to inter-individual differences in FMO3 phenotype [17–19]. In order to identify novel mutations of FMO3 and/or haplotypes of the *FMO3* gene found in Japanese individuals suffering from trimethylaminuria, we resequenced the entire coding region of the *FMO3* gene using genomic DNA from individuals that, judged by self-reported analysis were suspected to be positive for trimethylaminuria and later showed low FMO3 metabolic capacity on the basis of urine testing of TMAO levels. In a preliminary report [20], there were some FMO3 variants like Cys197Stop, Asp198Glu or Arg205Cys observed in a Japanese population, but the characterization of these FMO3 mutants were not examined in detail.

Herein, we report data supporting the involvement of two novel deleterious *FMO3* gene mutations causative of abnormal TMA *N*-oxygenation and trimethylaminuria in self-reporting Japanese individuals that were diagnosed with low FMO3 metabolic capacity based on urine testing. Subjects homozygous for either of the nonsense mutations, Arg500Stop and Cys197Stop alleles, in the *FMO3* gene suffered from trimethylaminuria.

Materials and methods

Chemicals

TMA and TMAO were obtained from Wako Pure Chemicals (Osaka, Japan). The tertiary amine substrate 10-[(*N*,*N*-dimethylaminopentyl)-2-(trifluoromethyl)]phenothiazene (5-DPT) and its *N*-oxide were synthesized as described previously [1,21]. The other chemicals and reagents used were obtained in the highest grade available commercially.

Subjects

The Ethics Committees of Showa Pharmaceutical University and Hokkaido University approved this study. Volunteer subjects who responded to an Internet article for screening of urinary TMA and TMAO levels and for sequencing the *FMO3* gene included 90 males and 74 females ranging from 1 to 64 years of age. Informed consent was obtained from each subject or parent. The study participants collected their urine samples as described previously [22]. Urinary TMA and TMAO concentrations were determined by gas chromatography using a flame ionization detector as described previously [23]. Urinary concentrations of free TMA or total TMA (μmol/mL of urine) were corrected for creatinine excretion (mmol/mL) [22]. Individuals that showed impaired FMO3 metabolic capacity, defined as the ratio of TMAO to total TMA (% of TMAO/(TMA + TMAO)), lower than 40% were considered to constitute abnormal TMA metabolism and possibly suffering from severe trimethylaminuria [16,22,24]. The values of urinary TMA and TMAO were shown as the average of at least three determinations obtained from first morning void urine.

DNA analysis

Genomic DNA prepared from peripheral lymphocytes [20] or buccal cells [25] of the study participants were analyzed. The sequence of the complete human *FMO3* gene described in GenBank (Accession Number AL021026) was used as a reference. Polymerase chain reaction (PCR) for the all exons and exon–intron junctions of the human *FMO3* gene was conducted in a 25 μL reaction mixture containing 50 ng of genomic DNA, 1.0 U LA-*Taq* DNA polymerase (Takarabio, Shiga, Japan), LA-PCR buffer, 2.0 mM $MgCl_2$, 0.2 mM dNTPs, 5.0 pmol of each sense and antisense primer reported previously [23]. The PCR conditions consisted of an initial denaturation at 94 °C for 1 min, followed by 35 cycles of denaturation at 94 °C for 30 s, annealing at 55 °C for 30 s, and extension at 72 °C for 45 s. The PCR products were directly sequenced on both strands using an ABI bigdye terminator cycle sequencing kit (Applied Biosystems, Foster City, CA, USA) with the sequencing primers [20]. The purified PCR products were analyzed on an ABI PRISM 3730*xl* DNA analyzer (Applied Biosystems).

Genotyping analysis for the novel g.30398 C > T mutation (Arg500Stop FMO3) in exon 9 was also carried out by a PCR-restriction fragment length polymorphism (RFLP) method with amplified DNA with the primers FMO3-9S and FMO3-9AS [23] and digestion by *Bss*SI at 37 °C for 2 h.

Recombinant wild-type and modified FMO3 protein preparations

The FMO3 cDNA used was previously modified by a PCR procedure [23] using a 5′-primer (5′-AAAAAGCTTACCATGGGGAAGAAAG-3′, that introduced an *Nco*I site prior to the start codon) and a 3′-primer (5′-CTAGAGAAGCTTATGATTAGGTCAACAC-3′, that introduced a *Hin*dIII site downstream of the stop codon). The full-length DNA sequence was confirmed again using DNA re-sequencing of both strands. To produce Arg205Cys FMO3, site-directed mutagenesis was performed by the primer-directed enzymatic amplification method [23]. Briefly, G-base at position 706 bp in the FMO3 cDNA was substituted by a T-base using the primers, 5′-AGAACTCAGCtGCACAGCAGA-3′ and 5′-TCTGCTGTGCaGCTGAGTTCT-3′, to introduce the single nucleotide substitution, that coded for Arg205Cys in exon 5. Similarly, a C-base at position 1590 bp was substituted by a T-base for preparation of Arg500Stop FMO3. The resultant cDNAs were amplified by KOD polymerase (Toyobo, Osaka, Japan). The wild-type and modified FMO3 cDNAs were introduced into the pTrc99A expression vector (Pharmacia Biotechnology, Milwaukee, MI, USA) and then transformed into *E. coli* strain JM109 as described previously [23]. The entire coding regions of the wild-type and mutagenized FMO3 cDNAs including the mutated sites were verified by re-sequencing of both strands.

Membrane fractions were prepared from the bacterial pellets that the FMO3 cDNAs had been introduced into by a series of fractionations and high-speed centrifugation steps as described previously [23]. Briefly, *E. coli* JM109 transformed by the FMO3 expression vector was grown overnight at 37 °C in Luria–Bertani medium containing 50 μg/mL ampicillin. A 1.0 mL aliquot of the starter culture was inoculated into 100 mL of Terrific Broth medium containing 50 μg/mL ampicillin, and 100 mM potassium phosphate buffer (pH 7.4) in a 300-mL triple-baffled flask and cultivated at 120 rpm at 30 °C. After the absorbance of the culture broth at a wavelength of 600 nm reached 0.3, 1 mM isopropyl-β-D-thiogalactoside was added and shaking was continued further for 24 h at 30 °C. The cells were then harvested by centrifugation at 10,000*g* for 20 min. All subsequent steps were carried out at 4 °C. The cells were resuspended (*ca.* 0.03 g/mL) in 50 mM Tris–acetate buffer (pH 7.5) containing 0.25 mM EDTA, 0.25 M sucrose, and 0.1 mg/mL lysozyme. The cell suspension was kept on ice for 30 min and then centrifuged at 9000*g* for 10 min. The pellet was resus-

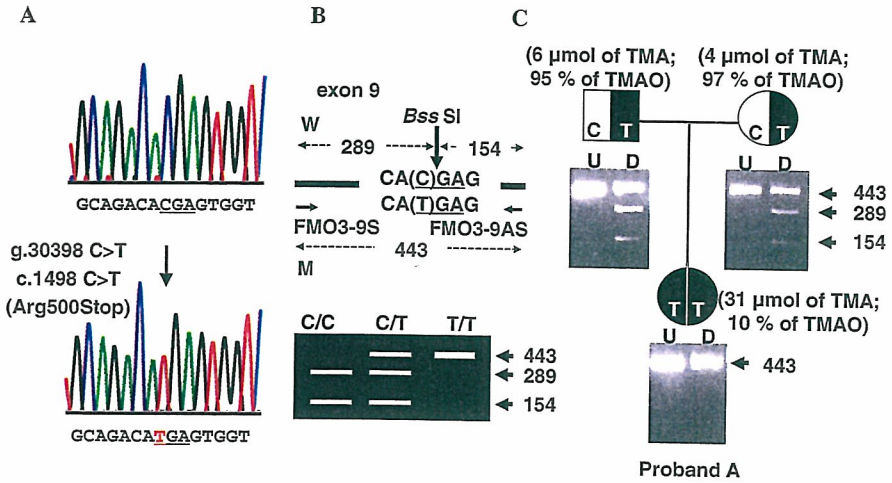

Fig. 1. (A) Nucleotide sequences of wild-type and variant of exon 9 of the *FMO3*. Both strands were sequenced. The sequences are shown only for sense strands for exon 9 of genomic DNA from the Proband A. (B) Genotyping analysis for the novel g.30398 C > T mutation (Arg500Stop FMO3) in exon 9 by PCR-RFLP with *Bss*SI. Genomic DNA was amplified with primers FMO3-9S and FMO3-9AS [23] and was digested by *Bss*SI. (C) Pedigree analysis for the presence of novel Arg500Stop mutation in the *FMO3* gene of the Proband A. The numbers in parentheses showed the results of both free TMA concentration (μmol TMA/mmol creatinine) and FMO3 metabolic capacity (% of TMAO to total TMA + TMAO) from analysis of urine. The PCR products before and after digestion with *Bss*SI were separated on 2 % agarose gel. U, uncut; D, digested with *Bss*SI.

pended (*ca.* 0.5 g/mL) in 100 mM potassium phosphate buffer (pH 7.4) containing 20% (v/v) glycerol, 6 mM magnesium acetate, 0.1 mM dithiothreitol, and 0.1 mM phenylmethylsulfonyl fluoride. Cells were disrupted using an ultrasonic processor and the resulting lysate was centrifuged at 9000*g* for 20 min. The supernatant was then further centrifuged at 100,000*g* for 1 h. The pellet (membrane fraction) was resuspended in one volume of 10 mM Tris–HCl buffer (pH 7.4) containing 0.1 mM EDTA and 20% glycerol (v/v). The amount of recombinant FMO3 was determined by immunoquantification by comparison with a standard of human FMO3 (BD Gentest, Woburn, MA, USA) and by the FAD content [23,26].

Wild-type human FMO3 and several truncated variants were also expressed in *E. coli* as maltose-binding fusion proteins using the expression vector pMAL-c2 [21,27]. The maltose-binding FMO3 proteins were purified by affinity chromatography as described previously [1,21,27].

Other assays

Rates of *N*-oxygenation of TMA and 5-DPT by recombinant FMO3 forms were determined by gas chromatography and HPLC, respectively, as described previously [23,27]. The methods yielded precision and accuracy of <10 % with linearity of time- (to 60 min) or protein- (to 1 mg/mL) dependent manner. The kinetic analysis of TMA *N*-oxygenation was performed using a nonlinear regression analysis program (KaleidaGraph, Synergy Software, Reading, PA, USA).

Results

DNA analysis of Proband A

FMO3 metabolic capacity was determined in self-reporting individuals that claimed to possess defective TMA *N*-oxygenation. Based on a low metabolic capacity of FMO3 (⩽40% urinary TMAO formation) causing severe trimethylaminuria symptoms [16,19], the frequency of subjects that showed less than 40% of FMO3 metabolic capacity was only 3.0% (5 individuals out of 164 individuals) in a Japanese population.

We focused on one of the participants that showed low metabolic capacity for TMA *N*-oxygenation (10–20%). From Proband A who showed 10 % FMO3 metabolic capacity, a single nucleotide substitution at g.30398 C > T in the *FMO3* gene was observed that resulted in c.1498C > T and caused a stop codon at Arg500 in exon 9 (Fig. 1A). The Proband A was homozygous for this novel FMO3 stop codon mutation. To confirm the mutation of this *FMO3* gene, a simple PCR-RFLP method was developed. As shown in Fig. 1B, the PCR product from the Arg500stop codon could not be digested by *Bss*SI. A more extensive analysis of DNA revealed that both parents of Proband A were heterozygous for the mutation at g.30398 C > T (Arg500Stop) (Fig. 1C). Analysis of urinary TMA *N*-oxygenation of both parents showed FMO3 metabolic capacity was greater than 90%, in contrast to 10 % metabolic capacity of Proband A (Fig. 1C).

DNA analysis of Proband B

We also observed the novel Arg500Stop mutation in the *FMO3* gene from Proband B that also possessed 21% metabolic capacity. In the course of sequencing the FMO3 DNA of the samples from this family (Fig. 2), we found that Proband B was heterozygous for the Arg500Stop allele and also had another allele (Fig. 2A) that was reported recently as a single nucleotide polymorphism [20]. The latter *FMO3* mutation was the g.21243_21244 TG deletion (c.591_592TG > del) caused a frameshift that encoded a new stop codon. This *FMO3* allele had g.5906 C > T and g.5907 A > G in intron 2, g.20852 C > T in exon 4 (c.441C > T), a g.20960_20962 CTT deletion, g.21115 G > A in intron 4, g.21246 T > A in exon 5 (c.594T > A), g.27091 C > T in exon 7 (c.855C > T), and a g.29232 T insertion in intron 8, together with the g.21243_21244 TG deletion in exon 5 (c.591_592TG > del) that coded for Cys197Stop.

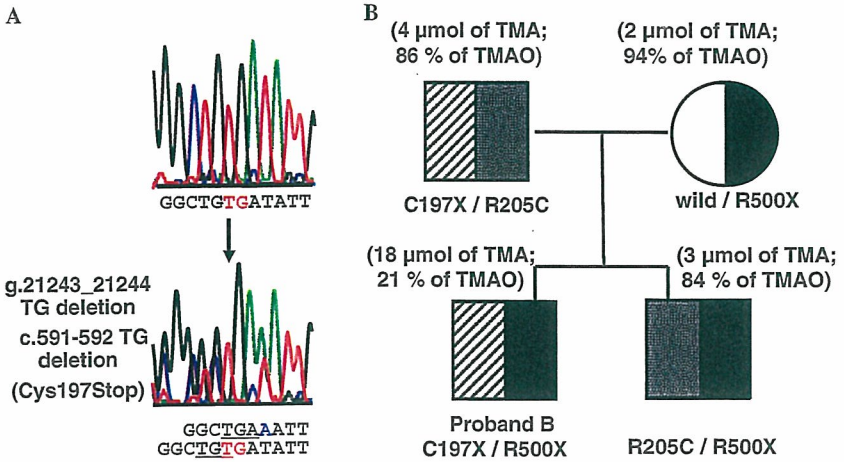

Fig. 2. (A) Nucleotide sequences of wild-type and variant of exon 5 of the *FMO3*. Both strands were sequenced. Antisense stands for exon 5 of genomic DNA from the Proband B are shown in a reversed manner, because of upstream deletions in sense strands. (B) A family study for Proband B who was heterozygous for Cys197Stop and Arg500Stop FMO3 mutations. See legend of Fig. 1 for details.

Other mutations

In addition, we found another haplotype containing g.21265 C>T in exon 5 (c.613C>T) from the father and brother of the Proband B that resulted in Arg205Cys FMO3 [20]. The individuals that were heterozygous for Arg205Cys FMO3 showed 84–86% of the FMO3 metabolic capacity *in vivo* (Fig. 2B). We recently reported two additional missense mutants, Thr201Lys FMO3 and Met260Val FMO3, as a preliminary single nucleotide polymorphism communication [28] from the other three subjects out of 164 individuals showing less than 40% FMO3 metabolic capacities.

The allelic frequencies of Cys197Stop, Arg205Cys, and Arg500Stop of the *FMO3* gene were estimated to be 2.1% (7 out of 328 alleles), 4.0% (13 out of 328 alleles), and 2.7% (9 out of 328 alleles), respectively, in this Japanese cohort. Additional Thr201Lys and Met260Val mutations showed less frequencies estimated to be 1.2% (4 out of 328 alleles) and 0.6% (2 out of 328 alleles), respectively, in the same cohort.

Recombinant Arg205Cys or Arg500Stop FMO3

Kinetic parameters for TMA *N*-oxygenation functional activity were determined by nonlinear regression analysis of recombinant Arg205Cys FMO3 and were compared with those of wild-type FMO3 expressed in bacterial membranes (Table 1). Apparent K_m values of wild-type and Arg205Cys FMO3 were not significantly different, but the V_{max} value of Arg205Cys was approximately one-fourth of that of wild-type enzyme.

To evaluate functional activity of the FMO3 mutant encoding a stop codon, recombinant Arg500Stop FMO3 was expressed in *E. coli* membranes and analyzed for functional activity. The Arg500Stop FMO3 expressed in the membranes was not able to catalyze *N*-oxygenation of TMA or another tertiary amine substrate for FMO3, 5-DPT (Table 2).

Table 1
Trimethylamine *N*-oxygenation activity of wild-type and Arg205Cys FMO3 cDNA expressed in *E. coli*

FMO3	Trimethylamine *N*-oxygenation activity	
	K_m (μM)	V_{max} (nmol products/min/nmol FMO3)
Wild-type	40 ± 8	16 ± 1
Arg205Cys	40 ± 5	4.2 ± 0.5

The *N*-oxygenation of trimethylamine (10–500 μM) was determined by gas chromatography.
Kinetic parameters were calculated from the fitted curve by nonlinear regression (means ± SE).

Table 2
Functional activity of wild-type and Arg500Stop FMO3 cDNA expressed in *E. coli*

FMO3	*N*-Oxygenation activity (nmol products/min/nmol FMO3)	
	Trimethylamine	5-DPT
Wild-type	14.1	2.1
Arg500Stop	<0.1	<0.01

The *N*-oxygenation of trimethylamine (100 μM) and 5-DPT (250 μM) were determined by gas chromatography and HPLC, respectively, in triplicate.
5-DPT, 10-[(*N*,*N*-dimethylaminopentyl)-2-(trifluoromethyl)]phenothiazene.

To further investigate the effects of stop codons on 5-DPT *N*-oxygenation, six highly purified FMO3 fusion proteins truncated at Phe510, Ser467, Leu437, Glu403, Asp339, and Glu305 were also studied. A series of highly purified FMO3 fusion proteins truncated at different positions (from Glu305 to Ser467) did not show any detectable enzymatic activities (<0.01 nmol products/min/nmol FMO3), except for Phe510Stop FMO3 that had *N*-oxygenation functional activity (0.02 nmol products/min/nmol FMO3) that was only 1% that of purified wild-type FMO3 fusion protein. These results collectively suggested that Cys197Stop FMO3 and Arg500Stop FMO3 possessed little

or no detectable functional activity as well, suggesting specific regions of the N-terminus of FMO3 was required for functional activity.

Discussion

The structural organization of the human *FMO3* gene has been reported [29]. Human *FMO3* is the gene candidate considered to be solely responsible for TMA *N*-oxygenation and deoderation and is defective in the inherited disorder, fish-like odor syndrome or trimethylaminuria. Because the functional FAD- and $NADP^+$-binding domains of the human *FMO3* (532 amino acids) are encoded by exon 2 and exon 5, respectively [29], it is possible that mutation(s) located toward the N-terminus of the *FMO3* could be responsible for decreased expression of the gene and/or abnormal functional activity or instability of the encoded protein. Previously, inactive variants of FMO3 at positions in exon 2 and exon 5 have been reported [8,9]. In the present study, a new mutation (Arg205Cys FMO3 in exon 5) was identified that possessed functional activity but decreased TMA *N*-oxygenase activity (Table 1). The frequency of this allelic variation may contribute to mild trimethylaminuria observed in the Japanese population, in association with a loss-of-function mutation on the other allele.

In addition, a novel Arg500Stop mutation (Fig. 1) responsible for severe trimethylaminuria was discovered in the Japanese population of the present study. Arg500Stop FMO3 encodes a 499 amino acid protein (out of 532 amino acids, or only 94% of the whole FMO3 structure). The Proband A that was a homozygote for this novel allele (Fig. 2) did not efficiently *N*-oxygenate dietary-derived TMA to TMAO. The observations about abnormal or impaired TMA *N*-oxygenation based on *in vivo* phenotype caused by the stop codon mutation in the *FMO3* gene was supported by *in vitro* evidence that showed no detectable functional activity of Arg500Stop FMO3 expressed in bacterial membranes (Table 2). Important contribution of C-terminus of human FMO3 for its function was clearly indicated but might be inconsistent with early findings of active recombinant FMO2 form in which the C-terminal 26 amino acids were deleted [30]. A molecular modeling of human FMO3 (532 amino acids) is worth examining to understand the contribution of C-terminus based on the recently reported crystal structure of yeast FMO (447 amino acids) [31], in spite of the low sequence identity (~20%) and short length (~80%) of the whole human FMO3 structure.

Furthermore, that no detectable functional activity of highly purified cDNA expressed FMO3 proteins truncated at several C-terminal positions was observed in this study suggests that the C-terminus of the human FMO3 is important for monooxygenation action. Taken together with the present results, the Cys197stop FMO3, found in Proband B (Fig. 2), should also be inactive for typical tertiary amine substrates.

The Japanese individuals did not possess any of the previously reported *FMO3* gene mutations that typically cause severe trimethylaminuria symptoms and low metabolic capacity of FMO3 ($\leqslant$40% urinary TMAO formation) [16,19]. We recently reported that relatively low FMO3 metabolic capacity associated with liver damage could be another causal factor for mild trimethylaminuria, independent of the *FMO3* genotype present [32]. On the other hand, the present study is the first report that the stop codons exist as mutants of *FMO3* in Japanese severe trimethylaminuria patients, although further studies are needed to be conducted to clarify whether or not these mutants and/or haplotypes are specific for Japanese suffering from trimethylaminuria. We recently reported two additional missense mutants, Thr201Lys FMO3 and Met260Val FMO3, as a preliminary single nucleotide polymorphism communication [28] from DNA of the other three subjects in this Japanese cohort showing less than 40% FMO3 metabolic capacities. Although these variants have not been fully characterized yet in terms of FMO3 function, recombinant Thr201Lys FMO3 and Met260Val FMO3 expressed in the bacterial membranes had impaired catalytic function in our preliminary study. Recently reported *FMO3* upstream variant haplotypes [33] and/or alternative processing [34] might also contribute to decreased *FMO3* expression and incidence of trimethylaminuria. Regardless, the present results suggest that truncation mutations of the *FMO3* gene that result in stop codons might be one of the causes of fish-like odor syndrome or trimethylaminuria in a Japanese cohort suffering from self-reported malodor, albeit at low frequencies (~2–4%). The frequency of these mutations should be low in healthy Japanese populations because they could not be found at all in approximately 100 alleles tested in control individuals (data not shown). The results from the present study also suggest that harboring at least one wild-type or decreased but not inactive allele of the *FMO3* gene could have FMO3 metabolic capacity and this may be relevant to diagnosis of trimethylaminuria.

In conclusion, individuals homozygous for either of the nonsense mutation Arg500stop or Cys197Stop alleles in the *FMO3* gene can possess abnormal TMA *N*-oxygenation and have trimethylaminuria. Heterozygotes for the nonsense mutations will exhibit trimethylaminuria symptoms only if they have, on the other chromosome, a mutation that substantially impairs enzyme activity (in which case they will have severe trimethylaminuria) or partially impairs enzyme activity (in which case they will have mild trimethylaminuria). The findings of the present study provide fundamental information for the importance of future investigations of the human *FMO3* gene associated with trimethylaminuria (fish-like odor syndrome).

Acknowledgments

We thank all of the volunteers for their participation in this study. We also thank Drs. Masaki Fujieda and Kazuma Kiyotani and Ms. Chihiro Yanagida for their help. This work was supported in part by the Ministry of

Education, Science, Sports and Culture of Japan, The Mochida Memorial Foundation for Medical and Pharmaceutical Research, and Japan Research Foundation for Clinical Pharmacology. J.R.C. was supported financially by a grant from NIH (Grant Number DK 59618).

References

[1] J.R. Cashman, B.R. Akerman, S.M. Forrest, E.P. Treacy, Population-specific polymorphisms of the human FMO3 gene: significance for detoxication, Drug Metab. Dispos. 28 (2000) 169–173.
[2] D.M. Ziegler, An overview of the mechanism, substrate specificities, and structure of FMOs, Drug Metab. Rev. 34 (2002) 503–511.
[3] D. Hernandez, A. Janmohamed, P. Chandan, I.R. Phillips, E.A. Shephard, Organization and evolution of the flavin-containing monooxygenase genes of human and mouse: identification of novel gene and pseudogene clusters, Pharmacogenetics 14 (2004) 117–130.
[4] N. Lomri, Q. Gu, J.R. Cashman, Molecular cloning of the flavin-containing monooxygenase (form II) cDNA from adult human liver, Proc. Natl. Acad. Sci. USA 89 (1992) 1685–1689.
[5] J. Zhang, J.R. Cashman, Quantitative analysis of FMO gene mRNA levels in human tissues, Drug Metab. Dispos. 34 (2006) 19–26.
[6] L.H. Overby, G.C. Carver, R.M. Philpot, Quantitation and kinetic properties of hepatic microsomal and recombinant flavin-containing monooxygenases 3 and 5 from humans, Chem. Biol. Interact. 106 (1997) 29–45.
[7] S.B. Koukouritaki, P. Simpson, C.K. Yeung, A.E. Rettie, R.N. Hines, Human hepatic flavin-containing monooxygenases 1 (*FMO1*) and 3 (*FMO3*) developmental expression, Pediatr. Res. 51 (2002) 236–243.
[8] D. Hernandez, S. Addou, D. Lee, C. Orengo, E.A. Shephard, I.R. Phillips, Trimethylaminuria and a human *FMO3* mutation database, Hum. Mutat. 22 (2003) 209–213.
[9] J. Zhang, Q. Tran, V. Lattard, J.R. Cashman, Deleterious mutations in the flavin-containing monooxygenase 3 (*FMO3*) gene causing trimethylaminuria, Pharmacogenetics 13 (2003) 495–500.
[10] S.B. Koukouritaki, R.N. Hines, Flavin-containing monooxygenase genetic polymorphism: impact on chemical metabolism and drug development, Pharmacogenomics 6 (2005) 807–822.
[11] S.C. Mitchell, R.L. Smith, Trimethylaminuria: the fish malodor syndrome, Drug Metab. Dispos. 29 (2001) 517–521.
[12] J.R. Cashman, J. Zhang, Interindividual differences of human flavin-containing monooxygenase 3: genetic polymorphisms and functional variation, Drug Metab. Dispos. 30 (2002) 1043–1052.
[13] E.P. Treacy, B.R. Akerman, L.M. Chow, R. Youil, C. Bibeau, J. Lin, A.G. Bruce, M. Knight, D.M. Danks, J.R. Cashman, S.M. Forrest, Mutations of the flavin-containing monooxygenase gene (*FMO3*) cause trimethylaminuria, a defect in detoxication, Hum. Mol. Genet. 7 (1998) 839–845.
[14] J.R. Cashman, K. Camp, S.S. Fakharzadeh, P.V. Fennessey, R.N. Hines, O.A. Mamer, S.C. Mitchell, G. Preti, D. Schlenk, R.L. Smith, S.S. Tjoa, D.E. Williams, S. Yannicelli, Biochemical and clinical aspects of the human flavin-containing monooxygenase form 3 (FMO3) related to trimethylaminuria, Curr. Drug Metab. 4 (2003) 151–170.
[15] S.C. Mitchell, Trimethylaminuria: susceptibility of heterozygotes, Lancet 354 (1999) 2164–2165.
[16] J. Zschocke, D. Kohlmueller, E. Quak, T. Meissner, G.F. Hoffmann, E. Mayatepek, Mild trimethylaminuria caused by common variants in *FMO3* gene, Lancet 354 (1999) 834–835.
[17] C.T. Dolphin, A. Janmohamed, R.L. Smith, E.A. Shephard, I.R. Phillips, Missense mutation in flavin-containing mono-oxygenase 3 gene, *FMO3*, underlies fish-odour syndrome, Nat. Genet. 17 (1997) 491–494.
[18] J.R. Cashman, Human flavin-containing monooxygenase (form 3): polymorphisms and variations in chemical metabolism, Pharmacogenomics 3 (2002) 325–339.
[19] J.R. Cashman, The implications of polymorphisms in mammalian flavin-containing monoloxygenases in drug discovery and development, Drug Discov. Today 9 (2004) 574–581.
[20] M. Fujieda, H. Yamazaki, M. Togashi, T. Saito, T. Kamataki, Two novel single nucleotide polymorphisms (SNPs) of the *FMO3* gene in Japanese, Drug Metab. Pharmacokinet. 18 (2003) 333–335.
[21] A. Brunelle, Y.A. Bi, J. Lin, B. Russell, L. Luy, C. Berkman, J. Cashman, Characterization of two human flavin-containing monooxygenase (form 3) enzymes expressed in *Escherichia coli* as maltose binding protein fusions, Drug Metab. Dispos. 25 (1997) 1001–1007.
[22] H. Yamazaki, M. Fujieda, M. Togashi, T. Saito, G. Preti, J.R. Cashman, T. Kamataki, Effects of the dietary supplements, activated charcoal and copper chlorophyllin, on urinary excretion of trimethylamine in Japanese trimethylaminuria patients, Life Sci. 74 (2004) 2739–2747.
[23] M. Kubota, Y. Nakamoto, K. Nakayama, P. Ujjin, S. Satarug, T. Mushiroda, T. Yokoi, M. Funayama, T. Kamataki, A mutation in the flavin-containing monooxygenase 3 gene and its effects on catalytic activity for *N*-oxidation of trimethylamine *in vitro*, Drug Metab. Pharmacokinet. 17 (2002) 207–213.
[24] A.Q. Zhang, S. Mitchell, R. Smith, Fish odour syndrome: verification of carrier detection test, J Inherit. Metab Dis. 18 (1995) 669–674.
[25] B. Richards, J. Skoletsky, A.P. Shuber, R. Balfour, R.C. Stern, H.L. Dorkin, R.B. Parad, D. Witt, K.W. Klinger, Multiplex PCR amplification from the CFTR gene using DNA prepared from buccal brushes/swabs, Hum. Mol. Genet. 2 (1993) 159–163.
[26] E.J. Faeder, L.M. Siegel, A rapid micromethod for determination of FMN and FAD in mixtures, Anal. Biochem. 53 (1973) 332–336.
[27] V. Lattard, J. Zhang, Q. Tran, B. Furnes, D. Schlenk, J.R. Cashman, Two new polymorphisms of the *FMO3* gene in Caucasian and African-American populations: comparative genetic and functional studies, Drug Metab. Dispos. 31 (2003) 854–860.
[28] M. Shimizu, H. Fujita, T. Aoyama, H. Yamazaki, Three novel single nucleotide polymorphisms of the *FMO3* gene in a Japanese population, Drug Metab. Pharmacokinet. 21 (2006) 245–247.
[29] C.T. Dolphin, J.H. Riley, R.L. Smith, E.A. Shephard, I.R. Phillips, Structural organization of the human flavin-containing monooxygenase 3 gene (FMO3), the favored candidate for fish-odor syndrome, determined directly from genomic DNA, Genomics 46 (1997) 260–267.
[30] M.P. Lawton, R.M. Philpot, Functional characterization of flavin-containing monooxygenase 1B1 expressed in *Saccharomyces cerevisiae* and *Escherichia coli* and analysis of proposed FAD- and membrane-binding domains, J. Biol. Chem. 268 (1993) 5728–5734.
[31] S. Eswaramoorthy, J.B. Bonanno, S.K. Burley, S. Swaminathan, Mechanism of action of a flavin-containing monooxygenase, PNAS 103 (2006) 9832–9837.
[32] H. Yamazaki, M. Fujieda, J.R. Cashman, T. Kamataki, Mild trimethylaminuria observed in a Japanese cohort with liver damage, Am. J. Med. 118 (2005) 803–805.
[33] S.B. Koukouritaki, M.T. Poch, E.T. Cabacungan, D.G. McCarver, R.N. Hines, Discovery of novel flavin-containing monooxygenase 3 (FMO3) single nucleotide polymorphisms and functional analysis of upstream haplotype variants, Mol. Pharmacol. 68 (2005) 383–392.
[34] V. Lattard, J. Zhang, J.R. Cashman, Alternative processing events in human *FMO* genes, Mol. Pharmacol. 65 (2004) 1517–1525.

Available online at www.sciencedirect.com
ScienceDirect
Biochemical and Biophysical Research Communications 352 (2007) 514–521
BBRC
www.elsevier.com/locate/ybbrc

Proteomics-based identification of biomarkers for predicting sensitivity to a PI3-kinase inhibitor in cancer

Tetsuyuki Akashi [a], Yumiko Nishimura [a], Rumi Wakatabe [b], Mieko Shiwa [b], Takao Yamori [a,*]

[a] *Division of Molecular Pharmacology, Cancer Chemotherapy Center, Japanese Foundation for Cancer Research, 3-10-6 Ariake, Koto-ku, Tokyo 135-8550, Japan*

[b] *Yokohama Laboratory, Ciphergen Biosystems K. K., Yokohama Business Park East Tower 14F, 134 Godo-cho, Hodogaya-ku, Yokohama, Kanagawa 240-0005, Japan*

Received 25 October 2006
Available online 20 November 2006

Abstract

To identify biomarkers for predicting sensitivity to phosphatidylinositol 3-kinase (PI3K) inhibitors, we have developed a proteomics-based approach. Using surface-enhanced laser desorption-ionization time-of-flight mass spectrometry (SELDI-TOF MS), we measured the expression of 393 proteins in 39 human cancer cell lines (JFCR-39), and combined it with our previously established chemosensitivity database to select for proteins whose expressions show significant correlations to drug sensitivities. This integrated approach allowed us to identify peaks from two proteins, 11.6 and 11.8 kDa, that showed significant correlations with the sensitivity to a PI3K inhibitor, LY294002. We found that the 11.8 kDa protein was a phosphorylated form of the 11.6 kDa protein. While the 11.8 kDa protein showed a positive correlation with the sensitivity to LY294002, the 11.6 kDa protein showed a negative correlation with that of the LY294002. The 11.6 kDa protein was purified chromatographically, and was identified by SELDI-TOF MS as the ribosomal P2 protein, which possesses two prospective phosphorylation sites. These results suggested that the phosphorylation status of the ribosomal P2 was responsible for determining the sensitivity to LY294002, and that the ribosomal P2 could be a potential biomarker for predicting chemosensitivity.
© 2006 Elsevier Inc. All rights reserved.

Keywords: SELDI-TOF MS; Proteomics; Biomarker; Prediction of chemosensitivity; Phosphorylation; Ribosomal P2

Characteristics of cancer cells vary from patients to patients, as they are transformed from various tissues and many types of physiological disorders contribute to their progress. Such variations cause differential response to anti-cancer drugs, thus resulting in a diversity of chemosensitivity in cancer cells. Accurate prediction of chemosensitivity in cancer therapy is particularly desirable in the clinic to avoid toxic side effects and to eliminate the use of any ineffective agent. Therefore, new biomarkers for predicting chemosensitivity are highly sought after to improve the current clinical capabilities, and the methodologies for the identification of potential biomarkers are in demand.

Panels consisting of human cancer cell lines coupled to a drug activity database are good models for investigating the diversity of chemosensitivity in cancer cells [1–3]. We have established a panel of 39 human cancer cell lines (termed JFCR-39 lines), and used this panel of cells to demonstrate that it provides a powerful means to predict the mechanism of drug action and identify new target compounds. For example, such integrative approaches have led to the identification of MS-247 [4], FJ5002 [5], and ZSTK474 [6] as target compounds for the topoisomerase I/II, telomerase, and phosphatidylinositol 3-kinase (PI3K), respectively. In addition, the panel of cells was used in combination with an array-based gene expression database to identify gene biomarker candidates for the prediction of chemosensitivity [7,8]. However, despite

* Corresponding author. Fax: +81 3 3570 0484.
E-mail address: yamori@jfcr.or.jp (T. Yamori).

0006-291X/$ - see front matter © 2006 Elsevier Inc. All rights reserved.
doi:10.1016/j.bbrc.2006.11.052

providing valuable and comprehensive data, the gene expression analysis method was not very useful in revealing any information on the post-translational modifications (such as phosphorylation, processing, glycosylation, acetylation, methylation, etc.) of the encoded proteins.

The recent development of proteomics-based technology has provided many tools for analyzing proteins from crude cell extracts. These new tools are expected to overcome the problem associated with the gene expression analysis technique. One such technology is surface-enhanced laser desorption-ionization time-of-flight mass spectrometry (SELDI-TOF MS). This technology uses protein chips made of a variety of chromatographic surfaces to selectively retain proteins from crude extracts, and provides a peak whose intensity is relatively quantitative and reproducible measure of a particular protein [9,10].

Our long-term goal is to identify protein biomarkers for predicting sensitivity to anti-cancer drugs. To identify the biomarkers, we comprehensively measured protein expression in the JFCR-39 lines by using the proteomics tool, SELDI-TOF MS, and combined it with our previous chemosensitivity database [3,4,6] to select proteins whose expressions show significant correlations to drug sensitivities. In the present study, we focused on LY294002 [11], one of the PI3K inhibitors, as a model of molecular-targeted drugs. The PI3K pathway is frequently activated in various types of cancer cells, and is believed to promote cell proliferation, growth, and survival [12,13]. Therefore, drugs targeted to PI3K are expected to be one of the efficient anti-cancer drugs [14,15]. Recently, several PI3K inhibitors have been developed for this purpose [6,16]. However, useful biomarkers determining chemosensitivity to PI3K inhibitors are currently unknown.

Here we report the finding of a biomarker candidate for the PI3K inhibitor LY294002 from an integrated database, and have identified the biomarker as the ribosomal P2 protein. Simultaneously, we have demonstrated that the SELDI-TOF MS can be used to isolate phosphoproteins from crude cell extracts. The identified ribosomal P2 may serve as a tool for predicting chemosensitivity.

Materials and methods

Cell lines and cell culture. The JFCR-39 [3] lines, used in this study, consist of the following 39 cancer cells: lung cancer, NCI-H23, NCI-H226, NCI-H522, NCI-H460, A549, DMS273, and DMS114; colorectal cancer, HCC-2998, KM-12, HT-29, HCT-15, and HCT-116; gastric cancer, St-4, MKN-1, MKN-7, MKN-28, MKN-45, and MKN-74; breast cancer, HBC-4, BSY-1, HBC-5, MCF-7, and MDA-MB-231; ovarian cancer, OVCAR-3, OVCAR-4, OVCAR-5, OVCAR-8, and SK-OV-3; glioma, U251, SF-268, SF-295, SF-539, SNB-75, and SNB-78; renal cancer, RXF-631L and ACHN; melanoma, LOX-IMVI; and prostate cancer, DU-145 and PC-3. All cell lines were cultured in RPMI 1640 supplemented with 5% fetal bovine serum, penicillin (100 U/ml), and streptomycin (100 μg/ml) at 37 °C in humidified air containing 5% CO_2.

Sample preparation for protein expression database. Cells were seeded at 1×10^6–6.8×10^6 cells in 100-mm dish and grown for 48 h at 37 °C. Cells were washed three times with cold PBS, scraped off the plate, and frozen in liquid N_2. Each frozen cell pellet was suspended in 800 μl of lysis buffer (50 mM Hepes–NaOH, pH 7.5, 0.5% Nonidet P-40, 1 mM sodium orthovanadate, 25 mM sodium fluoride, 15 mM pyrophosphate, and 5 mM EDTA) containing protease inhibitors (0.1 mM phenylmethylsulfonyl fluoride, 1 μg/ml leupeptin, and 1 μg/ml pepstatin) and incubated on ice for 30 min. After centrifugation at 20,000*g* for 20 min, the proteins in the supernatant were denatured by addition of solid urea, CHAPS, and DTT at the final concentration of 6 M, 2%, and 1 mM, respectively. Protein concentration was estimated using a Protein Assay Kit (Bio-Rad, Hercules, CA, USA) and adjusted to 1 mg/ml. All samples were stored at −80 °C.

Protein expression analysis on protein chips and data processing. Protein expression database of the samples was obtained by using strong anion-exchange (Q10), weak cation-exchange (CM10), immobilized affinity capture (IMAC30) charged with Ni^{2+} of protein chips (Ciphergen Biosystems, Fremont, CA, USA). Using a 96-well type bioprocessor, chips were pre-equilibrated two times with 200 μl of an appropriate binding buffer as follows: Q10 chip with 0.1 M Hepes–NaOH, pH 8.0, or 0.1 M sodium acetate, pH 5.0; CM10 chip with 0.1 M sodium phosphate, pH 7.0, or 0.1 M sodium acetate, pH 4.0; and IMAC30 chip with PBS. Each sample was diluted 1:1 in one of the binding buffers to 0.5 mg/ml and 50 μl of the diluted sample was applied to the respective chip. After incubation for 15 min at room temperature, the chips were washed three times with 200 μl of the respective binding buffer for 5 min and rinsed once with 200 μl of deionized water. Spots on the chips were allowed to dry, and each spot was twice treated with 0.5 μl of saturated sinapinic acid (SPA) or α-cyano-4-hydroxy cinnamic acid (CHCA) in 50% acetonitrile in water containing 0.5% trifluoroacetic acid. The protein chips were analyzed using the ProteinChip Biology System Reader (Model PBS II, Ciphergen) and the data were analyzed by ProteinChip Software version 3.2 (Ciphergen). All data were normalized using total ion current normalization function of the software.

Correlation analysis between protein expression and chemosensitivity databases. The chemosensitivity database was obtained by determining the 50% growth inhibition parameter (GI_{50}) for each drug as described previously [4,7]. The degree of correlation between the protein expression and drug activity was calculated using the following Pearson correlation coefficient formula: $r = \sum x_i(y_i - y_m)/\{\sum x_i^2(y_i - y_m)^2\}^{1/2}$, where x_i represents the expression of protein (peak intensity value) in cell i, y_i is the log sensitivity ($|\log_{10}GI_{50}|$) of cell i to drug y, and y_m represents the mean sensitivity ($|\log_{10}GI_{50}|$) of the drug. In this analysis, we selected the protein peak that passed the cut-off filter (peak intensity signal:noise ratio >10). We then selected the peaks where the protein expression patterns showed significant correlations to the drug activity patterns. A significant correlation was defined as having a $P < 0.005$ and a correlation coefficient $>|0.4|$.

Phosphatase treatment. Cells (A549), grown as above in 100-mm dish, were washed three times in cold PBS, scraped off from the dish, and then frozen in liquid N_2. The cell pellet was suspended in 800 μl of lysis buffer (50 mM Hepes–NaOH, pH 7.5, 0.5% Nonidet P-40) containing protease inhibitors (0.1 mM phenylmethylsulfonyl fluoride, 1 μg/ml leupeptin, and 1 μg/ml pepstatin) and incubated on ice for 30 min. After centrifugation at 20,000*g* for 20 min at 30 °C, the proteins in the supernatant were incubated in the reaction buffer (50 mM Hepes, pH 7.5, 0.1 mM EDTA, 5 mM DTT, and 0.01% Brij 35) with or without lambda protein phosphatase (λ-PPase; New England Biolabs, Beverly, MA, USA). The phosphatase reaction was inhibited by addition of phosphatase inhibitors (1 mM sodium orthovanadate, 25 mM sodium fluoride, and 15 mM pyrophosphate at final concentration).

Purification of biomarker candidates. Cellular proteins from the MKN-1 cells, extracted and denatured as described above, were diluted with an equal volume of the binding buffer (50 mM Hepes–NaOH, pH 7.5, 1 mM sodium orthovanadate, 25 mM sodium fluoride, and 15 mM pyrophosphate) and loaded onto to a Q-Sepharose column (GE Healthcare Bio-Sciences, Piscataway, NJ, USA), which was equilibrated with the same binding buffer. Proteins were eluted with 20 ml of a linear gradient buffer containing increasing NaCl concentration (from 180 to 380 mM) using a flow rate of 1 ml/min, the eluted proteins were collected in 1 ml fractions and were analyzed by SELDI-TOF MS using NP20 chips. Fractions

containing the 11.6, 11.7, and 11.8 kDa protein molecules were further purified using the reverse-phase chromatography on a RPC column (GE Healthcare Bio-Sciences). These proteins were eluted with a 36–40% acetonitrile gradient in 0.05% trifluoroacetic acid using a flow rate of 0.5 ml/min. Eluted proteins were fractionated and analyzed by SELDI-TOF MS using NP20 chips, selected fractions were concentrated using SpeedVac. The concentrated proteins were treated with λ-PPase to dephosphorylate phosphoproteins as described above, and were resolved by 16.5% SDS–PAGE. The gel was analyzed by silver-stain according to a manufacturer's instruction (Daiichi Pure Chemicals, Tokyo, Japan) or was stained with Coomassie brilliant blue to use for the protein identification process as described below.

Identification of biomarker candidates. Gel pieces containing the target 11.6 kDa protein were excised. The gel pieces were sequentially incubated as follows: three times with 50 μl of 50% acetonitrile in 50 mM ammonium bicarbonate, pH 8.0, on a shaker at room temperature for 10 min, one time with 500 μl of 50% acetonitrile in 50 mM ammonium bicarbonate, pH 8.0, for 30 min, and then one time with 50 μl of 100% acetonitrile for 15 min. After the final incubation, the gel pieces were dried by SpeedVac for 15 min. Trypsin (modified, sequencing grade; Roche Diagnostics, Basel, Switzerland) or V8 protease (Roche Diagnostics) in 50 mM ammonium bicarbonate, pH 8.0, was added and incubated for 16 h at 37 °C to digest the C-terminal of Arg/Lys or Glu, respectively. The reaction mixture was applied to NP20 chips and was allowed to air-dry. After drying, 20% saturated CHCA in 50% acetonitrile in water containing 0.5% trifluoroacetic acid was added. To identify the protein, the peptide digests were analyzed both by ProteinChip Biology System for the peptide fingerprint analysis and QSTAR Pulsar i (ABI, Foster, CA, USA) equipped with a PCI 1000 ProteinChip Array interface (Ciphergen) for the sequence tag analysis. Database searches were performed using Mascot search engine (Matrix Science, London, UK).

Results

Protein expression database for 39 human cancer cell lines using SELDI-TOF MS

To measure comprehensive protein expression in the JFCR-39 lines, a series of protein chips were used. The protein expression database was obtained by purification of proteins from each cell lysate using five different conditions (Q10 chip at pH 5.0 and 8.0, CM10 chip at pH 4.0 and 7.0, and IMAC-Ni) and subsequently detected by SELDI-TOF MS using two types of matrices, SPA and CHCA. The SPA was used for the mass-to-charge ratio (m/z) range of 8000–25,000, and the CHCA was used for the m/z range of 3000–10,000. After the acquisition of the protein expression database, we have chosen the protein peaks that passed the cut-off filter (peak intensity signal:noise ratio >10), and selected 393 peaks for further analysis (Supplemental Table 1a–g). The database consisted of the mass and signal intensity values for each peak.

Correlation analysis between protein expression and chemosensitivity databases

To screen for the biomarker candidates determining the chemosensitivity to LY294002, the protein expression database was integrated with the chemosensitivity database that was previously determined by measuring the growth inhibition parameters of LY294002 for the cells in the JFCR-39 lines. The growth inhibition parameter, which indicated sensitivity to the drug, for each cell was defined as the drug concentration (GI_{50}) that inhibits cell growth to 50%. After integration, we performed a correlation analysis between the two databases. For that purpose, we calculated the Pearson correlation coefficients for the 393 protein peaks and sensitivity to LY294002. We then selected the protein peaks that satisfied the following criteria: a significant correlation of $P < 0.005$ and a correlation coefficient of $>|0.4|$. Table 1 lists the 10 protein peaks (m/z), which showed significantly high correlation coefficient values. Notably, the peak with the highest correlation coefficient was the 11.6 kDa peak (11,648 m/z, $r = -0.634$, $P = 0.000015$). The 11.6 kDa protein was purified on a Q10 chip (at pH 8.0 condition) and detected using the SPA as matrix. The two 5.8-kDa peaks showing the second and third highest coefficient values (Table 1) were observed on the same type of chip (Q10). These peaks were considered to be evolved from the doubly charged 11.6 kDa protein. The 11.6 kDa protein peak showed a negative correlation ($r = -0.634$) with the sensitivity to LY294002, suggesting that a cell line expressing higher amounts of 11.6 kDa protein would be more resistant to LY294002 (Fig. 1A).

The raw mass spectrum for the 11.6 kDa peak is shown in Fig. 1B. We also noticed two other peaks, 11.7 kDa (11,729 m/z) and 11.8 kDa (11,808 m/z), respectively, near the 11.6 kDa peak. Interestingly, these two peaks showed a mass difference of 80 and 160 Da, respectively, from that of the 11.6 kDa peak (Fig. 1B). The 80 Da mass difference drew our attention because it is well known that phosphorylation of a peptide leads to an 80 Da shift in mass. Thus, we believe that the 11.7 and 11.8 kDa peaks represent single- and double-phosphorylated forms of the 11.6 kDa protein. More interestingly, the 11.8 kDa protein peak showed a positive correlation ($r = 0.543$, $P = 0.00035$) with the sensitivity to LY294002 (Fig. 1A, Table 1); this is in contrast to that of the 11.6 kDa protein peak, which showed a negative correlation with the sensitivity to LY294002. Taken together, these data suggested that a cell line expressing higher amounts of the 11.8 kDa protein would exhibit

Table 1
List of top 10 protein peaks showing high correlation with the sensitivity to LY294002

No.	m/z	Chip	pH	EAM	r	P
1	11,648	Q10	8	SPA	−0.634	0.000015
2	5827	Q10	8	CHCA	−0.613	0.000034
3	5824	Q10	5	CHCA	−0.562	0.0002
4	11,808	Q10	8	SPA	0.543	0.00035
5	5381	CM10	4	CHCA	−0.525	0.00059
6	3608	CM10	4	CHCA	−0.508	0.00097
7	5906	Q10	8	CHCA	0.499	0.0012
8	5415	CM10	4	CHCA	−0.499	0.0012
9	7130	Q10	8	CHCA	0.495	0.0014
10	7156	Q10	8	CHCA	0.488	0.0016

Note. m/z, chip, pH, EAM, r, and P represents the mass-to-charge ratio of each protein peak, the type of protein chip, pH condition during purification process, the type of matrix for ionization, correlation coefficient, and P value, respectively.